BOUNDARY LAYER SCALING IN RAYLEIGH-BÉNARD CONVECTION

Maarten van Reeuwijk[1], Harm Jonker[2] and Kemo Hanjalić[3]
[1] Imperial College London, London, United Kingdom
[2] Delft University of Technology, Delft, the Netherlands
[3] University of Rome "La Sapienza", Rome, Italy

Abstract

The scaling of the kinematic boundary layer thickness λ_u and the friction factor C_f at the top- and bottom-wall of Rayleigh-Bénard convection is studied by Direct Numerical Simulation (DNS). By a detailed analysis of the friction factor, a new parameterisation for C_f and λ_u is proposed. The simulations were made of an $L/H = 4$ aspect-ratio domain with periodic lateral boundary conditions at $\mathrm{Ra} = \{10^5, 10^6, 10^7\}$ and $\mathrm{Pr} = 1$. The best-fits of the simulations are $\lambda_u \propto \mathrm{Ra}^{-0.13}$ and $C_f \propto \mathrm{Ra}^{-0.3}$. By analysing the horizontal momentum equation, it is shown that the friction factor is dominated by the pressure gradient. Using a conceptual wind model, we find that the friction factor C_f should scale proportional to the thermal boundary layer thickness as $C_f \propto \lambda_\Theta$, while the kinetic boundary layer thickness λ_u scales inversely proportional to the thermal boundary layer thickness and wind Reynolds number $\lambda_u \propto \lambda_\Theta^{-1}\mathrm{Re}^{-1}$. The predicted trends for C_f and λ_u are in agreement with DNS results.

1 Introduction

The structure of the boundary layer is of great importance for understanding the turbulent heat transfer characteristics of Rayleigh-Bénard convection. Inherently unstable due to buoyancy effects, the thermal boundary layer with thickness λ_Θ is in a dynamic equilibrium of heating (cooling) by thermal diffusion and the detrainment (entrainment) of heat due to impinging and ejecting thermals at the bottom (top) plate. This process creates large temperature gradients across the boundary layer, thereby enhancing the heat transfer through the wall and thus the Nusselt number Nu. Next to a thermal boundary layer, one can identify a kinetic boundary layer with thickness λ_u, associated with the velocity field. Depending on the Prandtl number $\mathrm{Pr} = \nu\kappa^{-1}$, which is the ratio between the kinematic viscosity ν and thermal diffusivity κ, the kinetic boundary layer can be nested inside the thermal boundary layer or vice versa, which influences the effectiveness of the heat transfer as a function of the Rayleigh number Ra. The Rayleigh number Ra is defined as $\mathrm{Ra} = \beta g \Delta\Theta H^3(\nu\kappa)^{-1}$, where β is the thermal expansion coefficient, g the gravitational constant, $\Delta\Theta$ the temperature difference between the top and bottom plate and H the domain height. The scaling of λ_Θ and λ_u as a function of Ra and Pr are therefore of importance for proper prediction of the heat transfer.

In the theory of Grossmann & Lohse (2000), the wind velocity U and the boundary layer thicknesses λ_u and λ_Θ are central parameters, which are used to estimate the dissipation rates of kinetic energy and temperature variance in the bulk and the boundary layers. In the theory, λ_Θ and λ_u are defined as

$$\lambda_\Theta \propto H/(2\mathrm{Nu}), \tag{1}$$

$$\lambda_u \propto H\mathrm{Re}^{-1/2}. \tag{2}$$

Relation (2) can be obtained by non-dimensionalising the steady laminar two-dimensional Prandtl boundary layer equations (Schlichting & Gersten, 2000; Grossmann & Lohse, 2004), by which (2) follows immediately. While (1) holds excellently, the correspondence of (2) with

experiments (Xin *et al.*, 1996; Xin & Xia, 1997) and simulations (Kerr, 1996; Kerr & Herring, 2000) is less satisfactory. In particular, the measured Re dependence of λ_u is much weaker than predicted by (2) (see also Fig. 1a). Given the central role of λ_u in GL theory, it is desirable to improve (2) so that it better represents measurements and simulations.

In this paper, a new parameterisation of the kinetic boundary layer thickness λ_u and the friction factor C_f is proposed. Direct Numerical Simulation (DNS) of an aspect-ratio $W/L = 4$ rectangular domain at $\mathrm{Ra} = 10^5, 10^6, 10^7$ and $\mathrm{Pr} = 1$ has been performed to analyse the budget of horizontal momentum and other relevant properties of the boundary layer. Section 2 contains a brief overview about the code for DNS, the simulations and the wind-decomposition. The budget of horizontal momentum is calculated for each Ra. The results are discussed in section 3 and the governing boundary layer equation is shown to be the result of pressure, diffusion and Reynolds stress. Based on the boundary layer equations, the friction factor C_f can be decomposed in a contribution from pressure and one from the momentum flux, which is done in 4. It is shown that the friction factor is dominated by the pressure gradient, leading to a parameterisation of C_f in terms of the pressure gradient and λ_Θ. Using a recently proposed conceptual model for the wind of Rayleigh-Bénard convection (van Reeuwijk *et al.*, 2007), the pressure gradient can be expressed in terms of the wind velocity (section 5), which leads to an expression for C_f as $C_f \propto \lambda_\Theta$. Then, the universality of the velocity profile in the boundary layer is used to construct a scaling for λ_u which results in $\lambda_u \propto \lambda_\Theta^{-1}\mathrm{Re}^{-1}$. Concluding remarks are made in section 6.

2 Simulations

Direct simulation of Rayleigh-Bénard convection has been performed at $\mathrm{Ra} = \{10^5, 10^6, 10^7\}$ and $\mathrm{Pr} = 1$ in a $\Gamma = 4$ aspect-ratio domain. The code is based on a second-order variance-preserving finite-difference discretisation of the three-dimensional Navier-Stokes equations and is fully parallellised. For the simulations at $\mathrm{Ra} = 10^7$, a grid of 256^3 was used, which is of sufficient resolution to resolve the smallest turbulent scales, i.e. the Kolmogorov scale $\eta_K = (\nu^3/\varepsilon)^{1/4}$ and Corrsin scale $\eta_K = \mathrm{Pr}^{-1/2}\eta_K$. The top and bottom wall are rigid (no-slip) and of fixed temperature. At the side domain boundaries, periodic boundary conditions are applied. For each Ra, 400 independent realisations were obtained by performing 10 independent simulations and sampling the velocity and temperature field roughly twice every convective turnover time.

Similar to domains confined by sidewalls, a wind structure develops also in domains with lateral periodic boundary conditions. However, here the wind structure can be located anywhere in the domain since it is not kept in place by sidewalls. To extract the wind, symmetry-accounted ensemble-averaging is used (van Reeuwijk *et al.*, 2005), which aligns the wind structure in different realisations before averaging. In this way a wind structure can be identified unambiguously for these domains, by which a decomposition in wind and fluctuations becomes possible. The resulting average velocity and temperature (three-dimensional fields) are denoted respectively by $\widetilde{u}_i$ and $\widetilde{\Theta}$. The tildes are used to distinguish the conditional average from the standard (long-time, ensemble or plane) average $\overline{X}$ which is a function of z only. The symmetry-accounted average can be interpreted exactly as classical Reynolds-averaged results. For further simulation details we refer to van Reeuwijk *et al.* (2005, 2007).

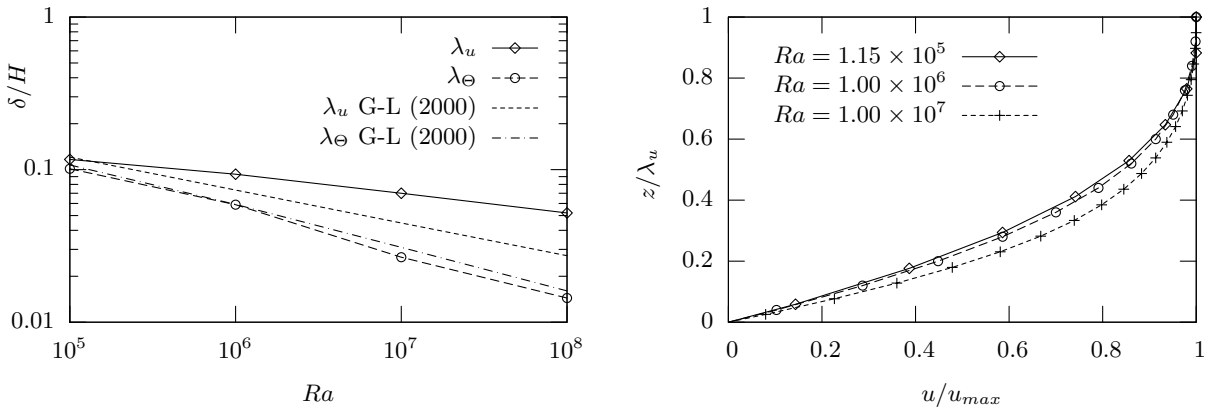

Figure 1: a) Thermal and kinematic boundary layer thickness as a function of Ra, together with the parameterisations from Grossmann & Lohse (2000). b) Velocity profile based on $\sqrt{\langle \widetilde{u}\ \widetilde{u} \rangle_A}$ in the boundary layer, non-dimensionalised by the maximum velocity $u_{\max}$ and the kinematic boundary layer thickness λ_u.

3 Boundary layer equations

Momentum budgets are a very direct way to get an impression of the importance of the turbulent Reynolds stresses. The horizontal momentum equation is given by

$$\partial_t \widetilde{u} \;=\; \underbrace{-\partial_j \widetilde{u}_j \widetilde{u}}_{\mathcal{A}} \;\; \underbrace{+\nu \partial_j^2 \widetilde{u}}_{\mathcal{D}} \;\; \underbrace{-\partial_x \widetilde{p}}_{\mathcal{P}} \;\; \underbrace{-\partial_j \widetilde{u_j' u_i'}}_{\mathcal{R}}, \tag{3}$$

where $\partial_t \widetilde{u} = 0$ as the system is statistically in steady state. For convenience of presentation, y-averaged results are used. Checks have been made to ensure that the budgets shown here are also representative for the three-dimensional field. The x-location has been chosen such that the horizontal velocity is at its maximum, i.e. where the flow is parallel to the wall and from left to right. This guarantees that horizontal gradients are small, and that no adverse of favourable pressure gradients are present. Shown is the budget of horizontal momentum at $\mathrm{Ra} = 1.15 \times 10^5$ (Fig 2a), $\mathrm{Ra} = 1.00 \times 10^6$ (Fig 2b) and $\mathrm{Ra} = 1.00 \times 10^7$ (Fig 2c). The budget has been nondimensionalized by $U^2/H = \beta g \Delta\Theta$, the z-coordinate has been re-scaled by the kinetic boundary layer λ_u and the horizontal dashed line denotes $z = \lambda_\Theta$. For the horizontal momentum budgets (Figs. 2a-c), the balance is between the horizontal pressure gradient $\mathcal{P}$, diffusion $\mathcal{D}$ for $z < \lambda_\Theta$; near $z = \lambda_u$, $\mathcal{P}$ is balanced by the Reynolds stresses $\mathcal{R}$. As the location of the budgets has been chosen such that all horizontal derivatives are small, $\mathcal{D} \approx \nu \partial_z^2 \widetilde{u}$ and $\mathcal{R} \approx -\partial_z \widetilde{w'u'}$. Outside the thermal boundary layer, $\mathcal{R}$ is not negligible; on the contrary, $\mathcal{R}$ fully balances the pressure gradient $\mathcal{P}$. This indicates that the turbulence outside the thermal boundary layer is key to the boundary layer thickness, as will be outlined in section 5.

The findings of Figs. 2a-c can be summarised as follows:

$$\partial_x \widetilde{p} + \partial_z \widetilde{w'u'} = \nu \partial_z^2 \widetilde{u}. \tag{4}$$

This is the boundary layer equation at the x-location where the flow is parallel to the wall and horizontal derivatives are negligible (roughly halfway between the impingement and detachment region). The presence of the Reynolds-stress term in (4) shows the importance of turbulence in the kinematic boundary layer. This may explain why the parameterisation $\lambda_u \propto \mathrm{Re}^{-1/2}$ in Grossmann & Lohse (2000, 2004) overpredicts the Ra dependence of λ_u: the parameterisation follows directly from the laminar boundary layer equations (Grossmann & Lohse, 2004) which do not hold for the entire kinematic boundary layer.

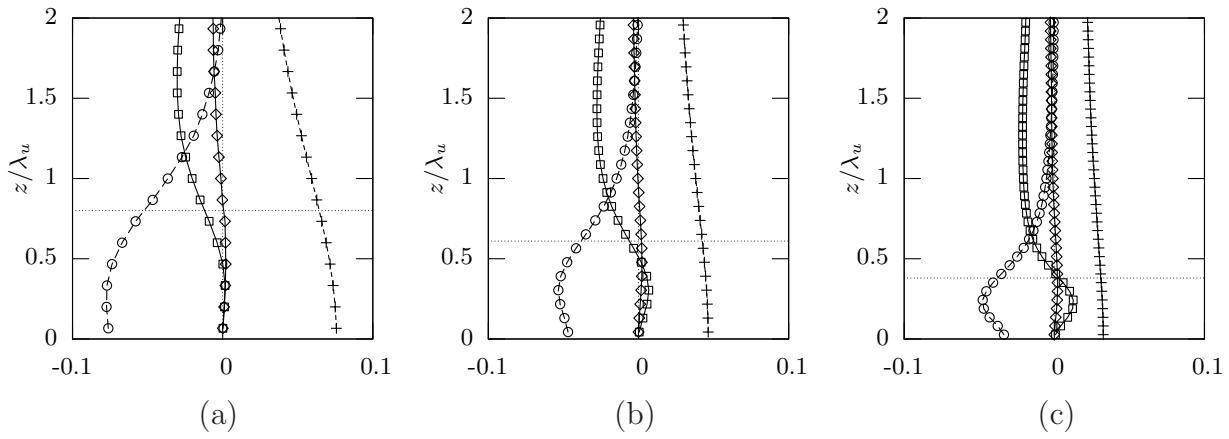

Figure 2: Momentum-budget in the boundary layer at the position with the maximum horizontal velocity for various Ra. a) Ra = 10^5; b) Ra = 10^6; c) Ra = 10^7. Shown are the pressure-gradient $\mathcal{P}$ (plusses), diffusion $\mathcal{D}$ (circles), advection by the mean flow $\mathcal{A}$ (diamonds) and Reynolds stress $\mathcal{R}$ (squares). The horizontal dashed line indicates the edge of the thermal boundary layer $z = \lambda_\Theta$.

4 Parameterisation of friction factor

The friction factor is one of the central parameters in boundary layer theory (Schlichting & Gersten, 2000) and is defined as

$$C_f = \frac{\tau_w}{\frac{1}{2}\rho u_{\max}^2}, \tag{5}$$

where τ_w is the wall-shear stress, and the denominator is the kinetic energy of the flow at the edge of the boundary layer. In Rayleigh-Bénard convection, the friction factor scales consistent with a laminar boundary layer as $C_f \propto \mathrm{Re}^{1/2}$ at moderate Rayleigh numbers (Chavanne *et al.*, 1997, 2001; Amati *et al.*, 2005), with a trend break towards a very low Re dependence of C_f consistent with a turbulent boundary layer beyond Ra = 10^{11} (Amati *et al.*, 2005; Niemela & Sreenivasan, 2006). The present simulations give values for C_f which are shown in Table 1 and a best-fit of $C_f = 0.2\mathrm{Re}^{-0.6}$.

By using the boundary layer equation (4), the dominant contributor to the wall friction term can be identified. Integrating (4) over the kinetic boundary layer and substituting (5), the friction factor C_f is composed of a contribution from pressure and a turbulent momentum flux as

$$\frac{C_f}{2} = \frac{1}{u_{\max}^2}\int_0^{\lambda_u} (\mathcal{P}+\mathcal{R})dz = -\frac{1}{u_{\max}^2}\int_0^{\lambda_u} \partial_x p dz - \frac{\widetilde{w'u'}|_{\lambda_u}}{u_{\max}^2}. \tag{6}$$

The terms on the right hand side of (6) have been calculated with the DNS results and are presented in Table 1. The decomposition clearly demonstrates that C_f is dominated by the pressure gradient. The turbulent momentum flux $\widetilde{w'u'}$ is small but positive, i.e. a flux out of the boundary layer. This behavior is not compatible with that of a forced turbulent boundary layer, where C_f is dominated by a large momentum-flux into the boundary layer, while the contribution of the pressure gradient is negligible.

Using (6), C_f can be parameterised. Recall that in the budget of horizontal momentum (Fig. 2), the force balance for $z < \lambda_\Theta$ is pressure $\mathcal{P}$ vs. diffusion $\mathcal{D}$, while for $z > \lambda_\Theta$ the Reynolds stress $\mathcal{R}$ balances the pressure $\mathcal{P}$. Hence, $\mathcal{P} + \mathcal{R} \approx \mathcal{P}$ for $z < \lambda_\Theta$ and $\mathcal{P} + \mathcal{R} \approx 0$ outside the thermal boundary layer, so that (5) can be approximated by

$$C_f \approx \frac{2\lambda_\Theta}{u_{\max}^2}\left|\partial_x p|_w\right|. \tag{7}$$

Table 1: Decomposition of the friction factor C_f according to (6)

Ra	$C_f =$	$-\frac{2}{u_{\max}^2}\int_0^{\lambda_u}\partial_x p dz$	$-\frac{2\widetilde{w'u'}\lvert_{\lambda_u}}{u_{\max}^2}$
10^5	0.81	0.88	-0.07
10^6	0.39	0.42	-0.03
10^7	0.17	0.19	-0.02

Here, $\partial_x p|_w$ is the pressure gradient at the wall. Clearly, (7) holds at moderate Ra only, when turbulent shear production in the boundary layer is small.

5 Scaling of C_f and λ_u

Using the simple two-equation wind model derived in van Reeuwijk *et al.* (2007), the pressure gradient of (7) can be related to the wind velocity, thereby establishing the scaling behavior of C_f and λ_u. The model is based on integration of the two-dimensional Reynolds-averaged Navier-Stokes equations over a suitable area within a single wind roll. The central parameters are the dimensionless wind-velocity $\hat{U}_w = U_w/U_f$ and spatial temperature difference $\hat{\Theta}_w = \Theta_w/\Delta\Theta$, where $U_f = \sqrt{\beta g \Delta\Theta H}$ is the free-fall velocity. The governing equations of the model are given by

$$\frac{d\hat{U}_w}{d\hat{t}} = \frac{2\hat{L}_w^2}{2\hat{L}_w^2+1}\left(\frac{1}{2\hat{L}_w}\hat{\Theta}_w - (4\alpha + C_f)\left|\hat{U}_w\right|\hat{U}_w\right), \tag{8}$$

$$\frac{d\hat{\Theta}_w}{d\hat{t}} = \frac{2\hat{\lambda}_\Theta}{\hat{L}_w}\hat{U}_w - \frac{4\alpha}{\hat{L}_w^2 \mathrm{Pr}_T}\left|\hat{U}_w\right|\hat{\Theta}_w - \frac{2}{\hat{\lambda}_\Theta \mathrm{Re}_f \mathrm{Pr}}\hat{\Theta}_w. \tag{9}$$

Here $\hat{L}_w = L_w/H$ where L_w is the typical roll size, $\hat{\lambda}_\Theta = \lambda_\Theta/H$, $\hat{\lambda}_u = \lambda_u/H$ and $\mathrm{Re}_f = U_f H/\nu = \mathrm{Ra}^{1/2}\mathrm{Pr}^{-1/2}$. The turbulent Prandtl number Pr_T and the mixing parameter α are coefficients with values 0.9 (Schlichting & Gersten, 2000) and 0.6 respectively. The model depends on Ra, Pr and $\hat{L}_w$, where $\hat{\lambda}_\Theta = \hat{\lambda}_\Theta(\mathrm{Ra},\mathrm{Pr})$ and $C_f = C_f(\mathrm{Ra},\mathrm{Pr})$ have to be provided.

The pressure difference which drives the wind is generated by a spatial temperature difference Θ_w (it is relatively hot where the flow ascends and relatively cold where it descends). The temperature difference Θ_w is in its turn generated by large horizontal heat fluxes originating from the interaction between the mean wind and temperature field. Ultimately, it is this heat-flux which is responsible for the generation of a large-scale wind.

Based on the analysis of the friction factor, an explicit expression for C_f can be derived, by which the model only depends on empirical input for $\hat{\lambda}_\Theta$ (and thus Nu). The steady state estimate for the pressure gradient at the bottom wall of the wind model is (van Reeuwijk *et al.*, 2007)

$$-\partial_x\widetilde{p}|_w \approx \frac{\beta g H}{L_w}\Theta_w. \tag{10}$$

Using (10), C_f (7) can be further specified as

$$C_f \approx \frac{2\lambda_\Theta}{H}\frac{H}{L_w}\frac{U_f^2}{U_w^2}\frac{|\Theta_w|}{\Delta\Theta} = \frac{2\hat{\lambda}_\Theta\left|\hat{\Theta}_w\right|}{\hat{L}_w\hat{U}_w^2}. \tag{11}$$

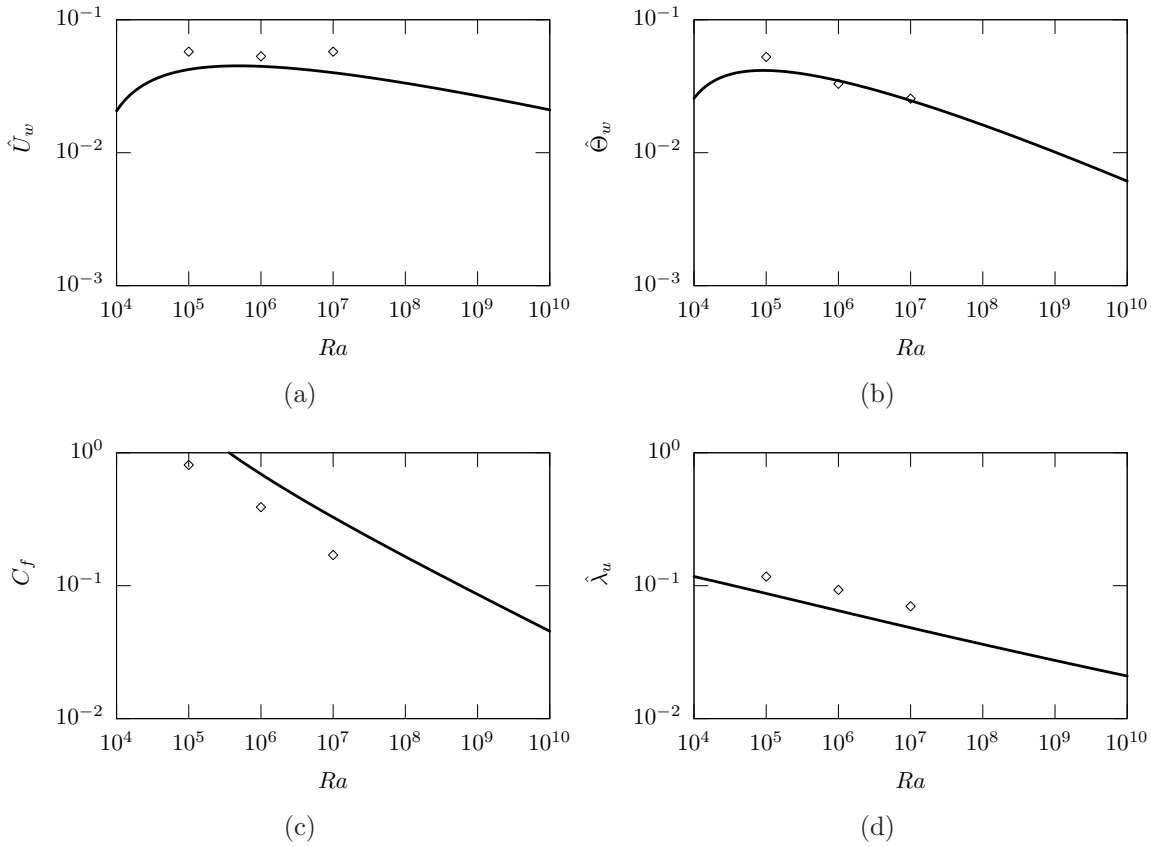

Figure 3: The predictions of the wind model (eqns (13), (14), thick solid line) compared to the DNS results (diamonds). a) the typical wind $\hat{U}_w$; b) the spatial temperature difference $\hat{\Theta}_w$; c) the friction factor C_f and d) kinetic boundary layer thickness λ_u.

Hence, the wall friction term is linear in the temperature difference as

$$C_f \left|\hat{U}_w\right| \hat{U}_w = \frac{2\hat{\lambda}_\Theta}{\hat{L}_w}\hat{\Theta}_w, \tag{12}$$

where it was assumed that sgn $\hat{U}_w$ = sgn $\hat{\Theta}_w$. With (12), the empirical specification of $C_f(\mathrm{Ra}, \mathrm{Pr})$ is no longer necessary, and the model is given by:

$$\frac{d\hat{U}_w}{d\hat{t}} = \frac{2\hat{L}_w^2}{2\hat{L}_w^2 + 1}\left(\frac{1 - 4\hat{\lambda}_\Theta}{2\hat{L}_w}\hat{\Theta}_w - 4\alpha\left|\hat{U}_w\right|\hat{U}_w\right), \tag{13}$$

$$\frac{d\hat{\Theta}_w}{d\hat{t}} = \frac{2\hat{\lambda}_\Theta}{\hat{L}_w}\hat{U}_w - \frac{4\alpha}{\hat{L}_w^2 \mathrm{Pr}_T}\left|\hat{U}_w\right|\hat{\Theta}_w - \frac{2}{\hat{\lambda}_\Theta \mathrm{Re}_f \mathrm{Pr}}\hat{\Theta}_w. \tag{14}$$

The steady state solution of the model as a function of Ra is shown in Fig. 3. At this point, the only empirical data used in the model is the powerlaw for λ_Θ and the roll size L_w. As can be seen, the model captures the trends of $\hat{U}_w$, $\hat{\Theta}_w$ and C_f satisfactorily. The profiles could be made to match quantitatively as well when one would introduce some additional coefficients. However, the focus of this paper is not to develop a carefully tuned model, but to elicit general scaling behavior.

It is not very useful to have an expression for C_f in terms of $\hat{\Theta}_w$, as this quantity is rarely measured. However, by using the steady state solution of (13), the $\hat{\Theta}_w$ dependence of C_f can be eliminated. Specifically, $\hat{\Theta}$ can be expressed in terms of $\hat{U}_w$ as

$$\hat{\Theta}_w = \frac{8\alpha\hat{L}_w}{1 - 4\hat{\lambda}_\Theta}\left|\hat{U}_w\right|\hat{U}_w, \tag{15}$$

Using (11) and (15), C_f becomes

$$C_f \approx \frac{16\alpha\hat{\lambda}_\Theta}{1-4\hat{\lambda}_\Theta}. \tag{16}$$

Hence, when $\hat{\lambda}_\Theta \ll 1$, the model predicts that $C_f \propto \hat{\lambda}_\Theta$. Note that the λ_Θ term in the denominator represents the effects of wall friction. Hence, when $\hat{\lambda}_\Theta \ll 1$, C_f scales *independently* of wall-effects. It is the turbulence in the outer flow which fully determines the velocity at the edge of the boundary layer.

A scaling relation for λ_u can be derived by using the near universality of the velocity profile in the boundary layer upon scaling by the velocity at the edge of the boundary layer $u_{\max}$ and λ_u (Fig. 1b). The universality implies that $\tau_w/\rho \approx \nu u_{\max}/\lambda_u$. As $\tau_w/\rho = \frac{1}{2}C_f u_{\max}^2$, a second expression for C_f is

$$C_f = \frac{2\nu}{u_{\max}}\frac{1}{\lambda_u} = 2\mathrm{Re}^{-1}\left(\frac{\lambda_u}{H}\right)^{-1}.$$

By relating the above expression for C_f to (11) and using $\mathrm{Re} = \left|\hat{U}_w\right| \mathrm{Re}_f$, $\hat{\lambda}_u$ is approximated by

$$\hat{\lambda}_u \approx \frac{\hat{L}_w\left|\hat{U}_w\right|}{\hat{\lambda}_\Theta\left|\hat{\Theta}_w\right|\mathrm{Re}_f} \tag{17}$$

Assuming that $\mathrm{sgn}\,\hat{U}_w = \mathrm{sgn}\,\hat{\Theta}_w$ and using (15), $\hat{\lambda}_u$ is given by

$$\hat{\lambda}_u \approx \frac{1-4\hat{\lambda}_\Theta}{8\alpha\hat{\lambda}_\Theta\hat{U}_w\mathrm{Re}_f} = \frac{1-4\hat{\lambda}_\Theta}{8\alpha\hat{\lambda}_\Theta\mathrm{Re}}. \tag{18}$$

Upon assuming that $\hat{\lambda}_\Theta \ll 1$, it follows that $\hat{\lambda}_u$ scales as $\hat{\lambda}_u \propto \hat{\lambda}_\Theta^{-1}\mathrm{Re}^{-1}$. Fig. 3d shows the prediction of the wind model for λ_u. Although the boundary layer thickness is underpredicted, the trend is in agreement with the DNS data. Given the simplicity (with only one calibration parameter α), the model captures the trends of wind velocity, spatial temperature difference, friction factor and kinetic boundary layer thickness satisfactorily.

6 Concluding remarks

In this paper, we used DNS to develop scaling laws for the kinematic boundary layer in Rayleigh-Bénard convection. Direct numerical simulation was used for simulations at $\mathrm{Ra} = \{10^5, 10^6, 10^7\}$ and $\mathrm{Pr} = 1$ for $\Gamma = 4$ aspect ratio domains with periodic lateral boundary conditions. For each Ra, 10 independent simulations have been carried out, resulting in approximately 400 independent realizations per Ra. Processing the results using symmetry-accounting ensemble averaging made it possible to retain the wind structure, which would normally cancel out due to the translational invariance of the system.

Using the simple conceptual wind model of van Reeuwijk *et al.* (2007), a scaling relation for C_f and λ_u was proposed. It was found that the friction factor should scale proportional to the thermal boundary layer thickness as $C_f \propto \lambda_\Theta$. The kinetic boundary layer thickness λ_u should scale inversely proportional to the thermal boundary layer thickness and the Reynolds number as $\lambda_u \propto \mathrm{Re}^{-1}\lambda_\Theta^{-1}$. The predicted trends for C_f and λ_u are in agreement with the DNS results. With the closure for C_f, the wind model (13), (14) depends solely on empirical input for λ_Θ, and predicts the wind Reynolds number Re, friction factor C_f and kinetic boundary layer thickness λ_u.

Further research is needed to verify the range of validity of the proposed scalings for C_f and λ_u. In particular, simulations with sidewalls and at lower Γ should be carried out. Another

interesting area of research is the scaling in boundary layers of low-Prandtl number convection, where $\lambda_u < \lambda_\Theta$.

Acknowledgments

The supercomputing facilities have been provided by the National Computing Facilities Foundation (NCF) and sponsored by the Netherlands Organization for Scientific Research (NWO).

References

Amati, G., Koal, K., Massaioli, F., Sreenivasan, K. R. & Verzicco, R. 2005 Turbulent thermal convection at high Rayleigh numbers for a Boussinesq fluid of constant Prandtl number. *Phys. Fluids* **17** (12), 121701.

Chavanne, X., Chilla, F., Castaing, B., Hebral, B., Chabaud, B. & Chaussy, J. 1997 Observation of the ultimate regime in Rayleigh-Bénard convection. *Phys. Rev. Lett.* **79** (19), 3648–3651.

Chavanne, X., Chilla, F., Chabaud, B., Castaing, B. & Hebral, B. 2001 Turbulent Rayleigh-Bénard convection in gaseous and liquid he. *Phys. Fluids* **13** (5), 1300–1320.

Grossmann, S. & Lohse, D. 2000 Scaling in thermal convection: a unifying theory. *J. Fluid Mech.* **407**, 27–56.

Grossmann, S. & Lohse, D. 2004 Fluctuations in turbulent Rayleigh-Bénard: The role of plumes. *Phys. Fluids* **16** (12), 4462–4472.

Kerr, R. M. 1996 Rayleigh number scaling in numerical convection. *J. Fluid Mech.* **310**, 139–179.

Kerr, R. M. & Herring, J. R. 2000 Prandtl number dependence of Nusselt number in direct numerical simulations. *J. Fluid Mech.* **419**, 325–344.

Niemela, J. J. & Sreenivasan, K. R. 2006 Turbulent convection at high Rayleigh numbers and aspect ratio 4. *J. Fluid Mech.* **557**, 411–422.

van Reeuwijk, M., Jonker, H. J. J. & Hanjalić, K. 2005 Identification of the wind in Rayleigh-Bénard convection. *Phys. Fluids* **17** (5), 051704.

van Reeuwijk, M., Jonker, H. J. J. & Hanjalić, K. 2007 Wind and boundary layers in Rayleigh-Bénard convection. i: analysis and modelling. *Accepted for Phys. Rev. E* .

Schlichting, H. & Gersten, K. 2000 *Boundary layer theory*. McGraw-Hill.

Xin, Y. B. & Xia, K. Q. 1997 Boundary layer length scales in convective turbulence. *Phys. Rev. E* **56** (3), 3010–3015.

Xin, Y. B., Xia, K. Q. & Tong, P. 1996 Measured velocity boundary layers in turbulent convection. *Phys. Rev. Lett.* **77** (7), 1266–1269.